Supporting information

Synergistic Dual-Interface Modification for High-Performance $CsPbBr_3$ Perovskite Solar Cells: A Combined Experimental and Modeling Study

Xinghua Li[1,2], Zhongchen Bai[3*], Qixin Chen[1,4], Zhengping Zhang[1*]

[1] College of Big Data and Information Engineering, Guizhou University, Guiyang City,550025, China

[2] College of Electronics and Information Engineering, Anshun University, Anshun City,561000, China

[3] College of Medicine, Guizhou University, Guiyang City, 550025, China

[4]Guizhou Polytechnic of Construction, Guiyang City,551499, China

*Correspondence: zcbai@gzu.edu.cn (Z.C. Bai),zpzhang@gzu.edu.cn (Z.P. Zhang).

List of Supplementary Items

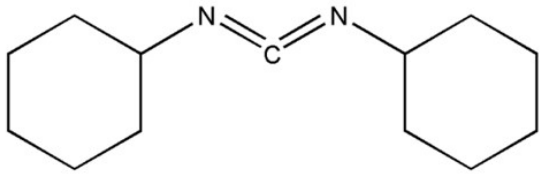

Fig. S1 N, N'-Dicyclohexylcarbodiimide (DCC)

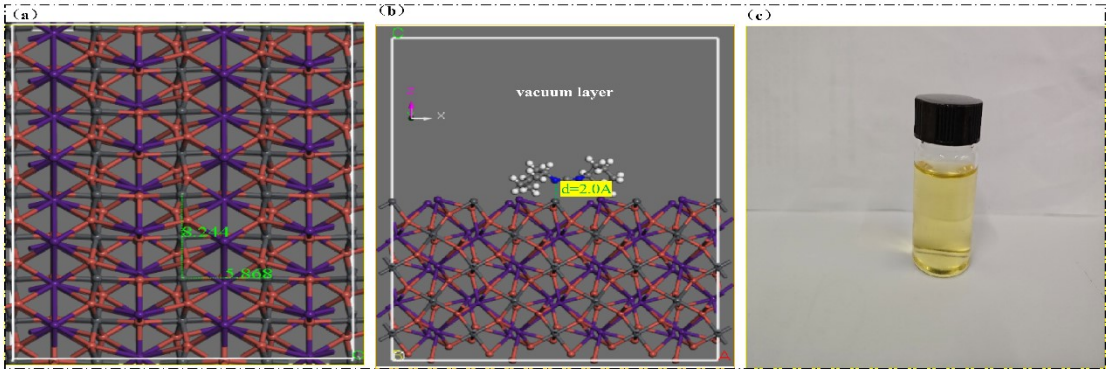

Fig. S2 (a) Model of DCC adsorbed on the $CsPbBr_3$ surface; (b) Pb–Pb interatomic distances on the $CsPbBr_3$ (001) surface; (c) SnO_2 quantum dots.

Supplementary Note 1

The $CsPbBr_3$(001) surface was modeled using a (4×3×1) supercell, with a slab thickness of 20 Å and a vacuum layer of 20 Å. The bottom three atomic layers were fixed, and the surface was terminated with $PbBr_2$. All calculations were performed using Material Studio.

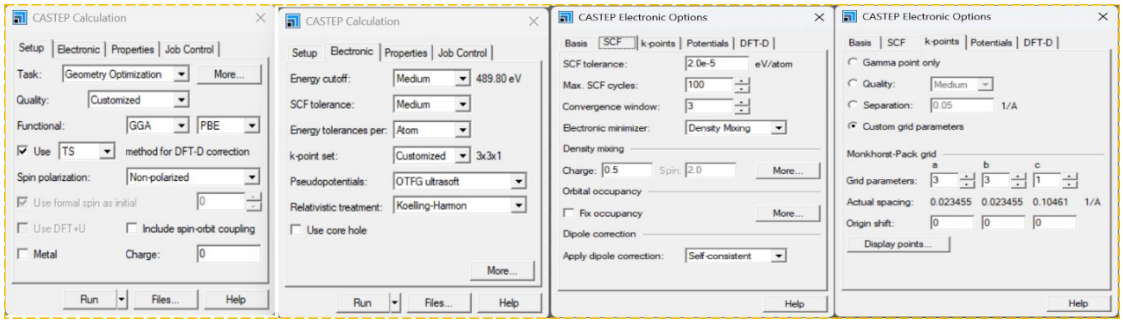

Fig. S3 Parameter settings for Geometry Optimization of DCC adsorbed on $CsPbBr_3$

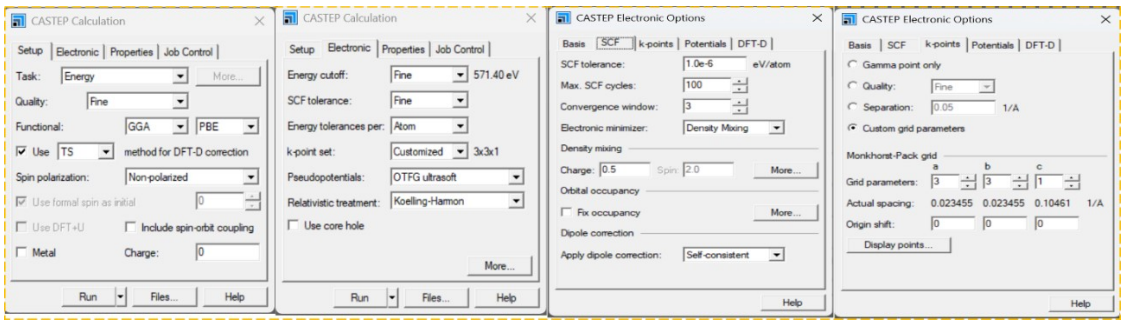

Fig. S4 Parameter settings for Energy of DCC adsorbed on $CsPbBr_3$

For the key parameter settings of structure optimization in Fig. S3, the GGA-PBE functional is

adopted. Considering computational performance, ultrasoft pseudopotentials are selected. The self-consistent field (SCF) convergence threshold is set to 10^{-5}, with the key point being the activation of the DFT-D dispersion correction. $CsPbBr_3$ is a “soft” lattice material, and the stability of its crystal structure largely depends on nonlocal dispersion interactions between Pb^{2+} and Br^- ions, as well as between different octahedral layers. With the inclusion of the dispersion correction, the lattice constants become more consistent with experimental values. For the single-point energy calculation in Fig. S4, the parameter settings are the same as those for structure optimization, except that the SCF precision is increased by a factor of 10 to 10^{-6}.

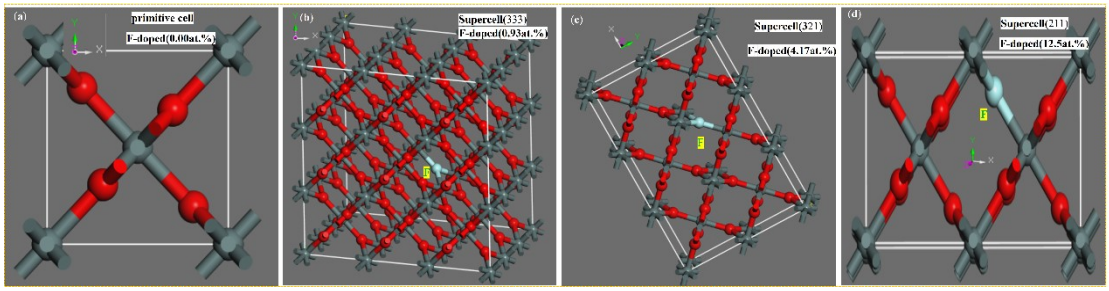

Fig. S5 Construction of SnO_2-F doping models with different concentrations

Table S1 DFT (CASTEP) parameter settings for SnO_2/SnO_2-F

Geometry Optimization/Energy				
Supercell	(1×1×1) F-doped(0.0at.%)	(2×1×1) F-doped(12.5at.%)	(3×2×1) F-doped(4.17at.%)	(3×3×3) F-doped(0.93at.%)
Quality	fine	fine	fine	fine
Cutoff	571.4	571.4	571.4	571.4
Pseudop	OTfG ultrasoft	OTfG ultrasoft	OTfG ultrasoft	OTfG ultrasoft

otentials				
Functionl	GGA PBE	GGA PBE	GGA PBE	GGA PBE
K-point	(6×6×4)	(3×6×4)	(2×3×4)	(2×2×2)
SCF	Geometry Optimization :1.0e-5 Energy: 1.0e-6	Geometry Optimization :1.0e-5 Energy: 1.0e-6	Geometry Optimization :1.0e-5 Energy: 1.0e-6	Geometry Optimization :1.0e-5 Energy: 1.0e-6

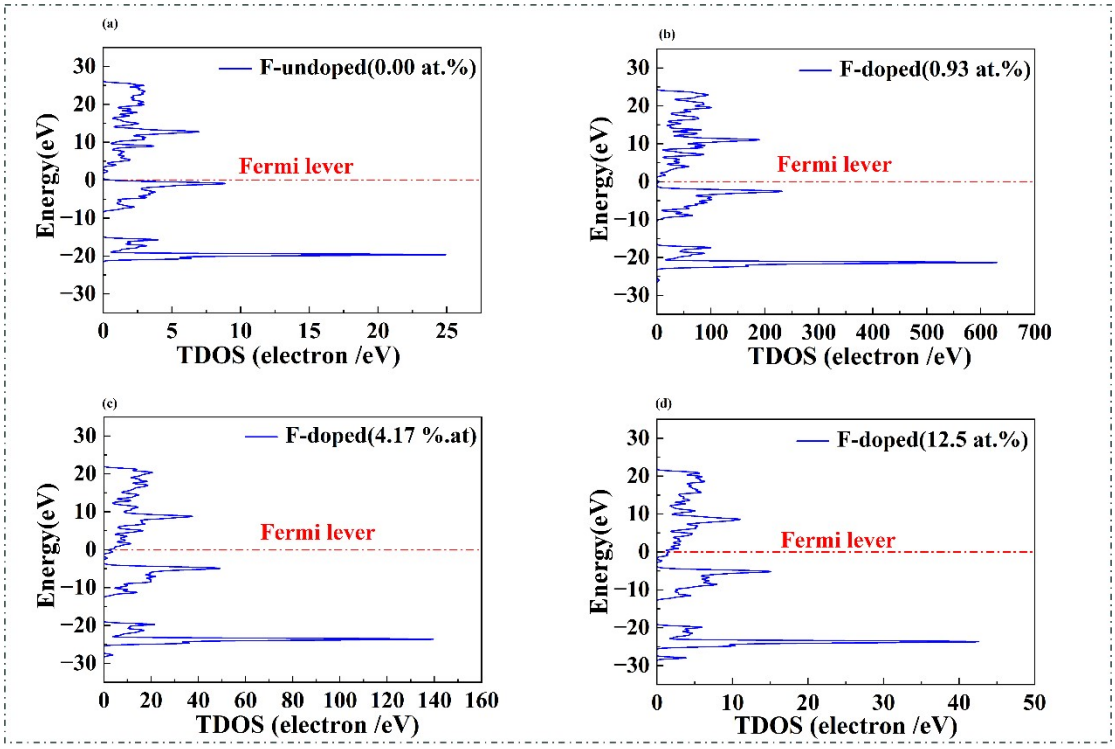

Fig. S6 TDOS

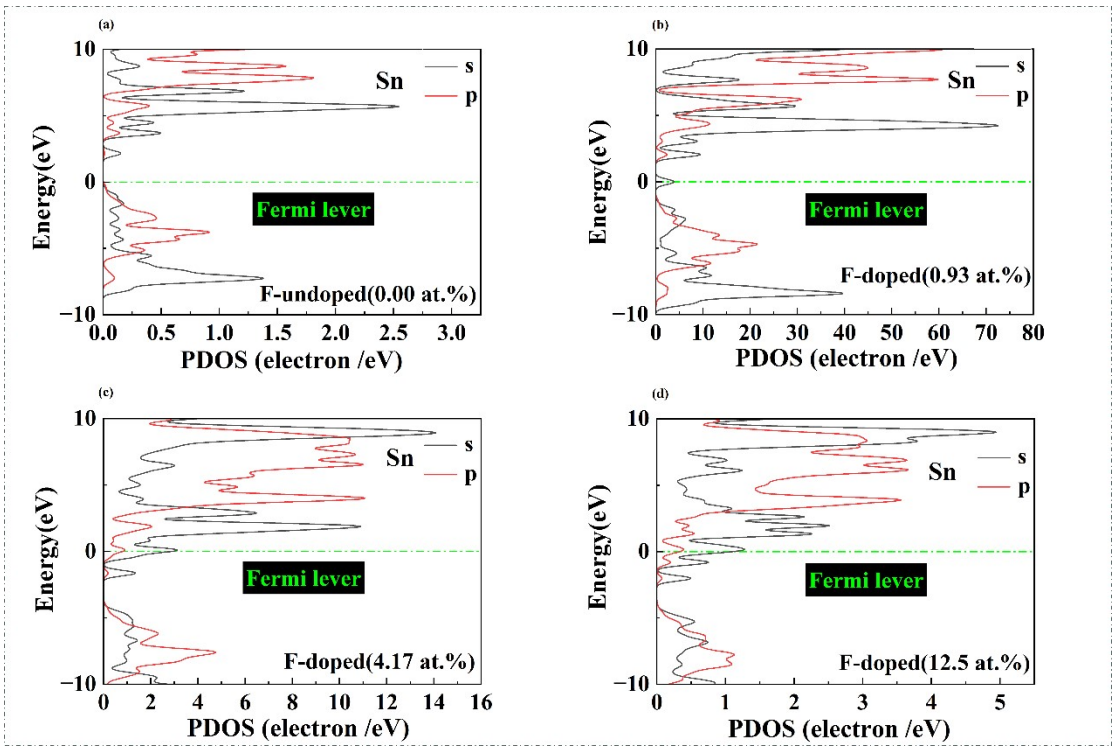

Fig. S7 Sn-PDOS

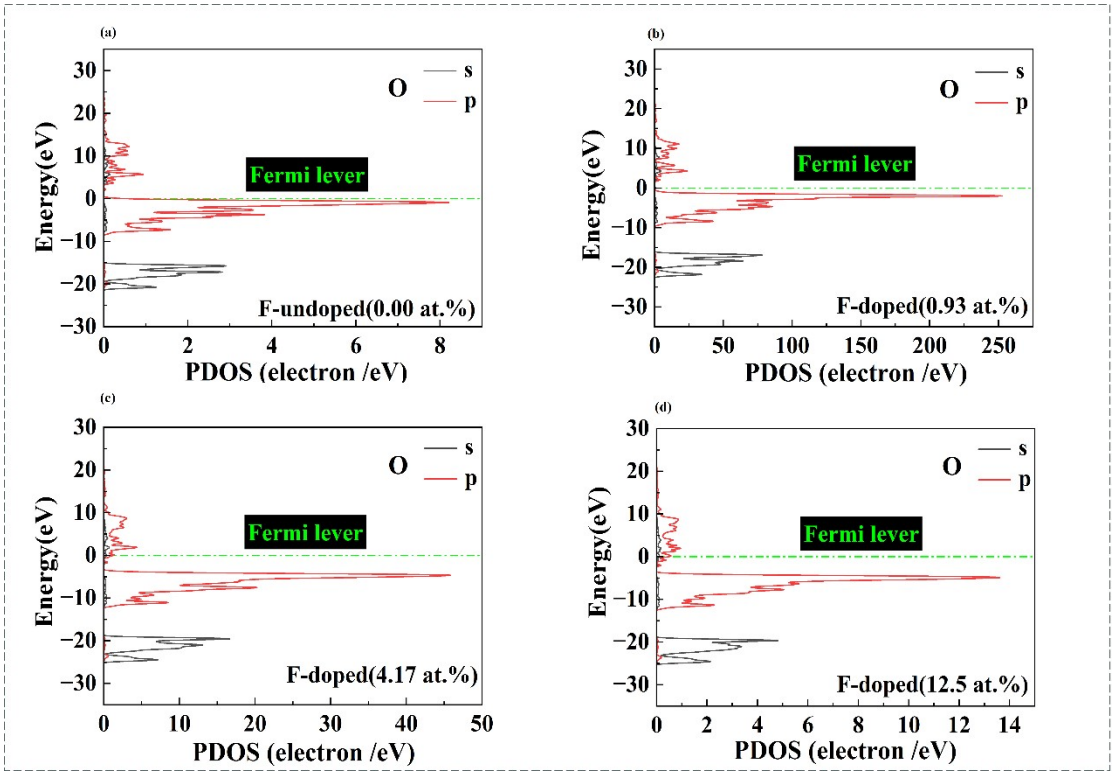

Fig. S8 O-PDOS

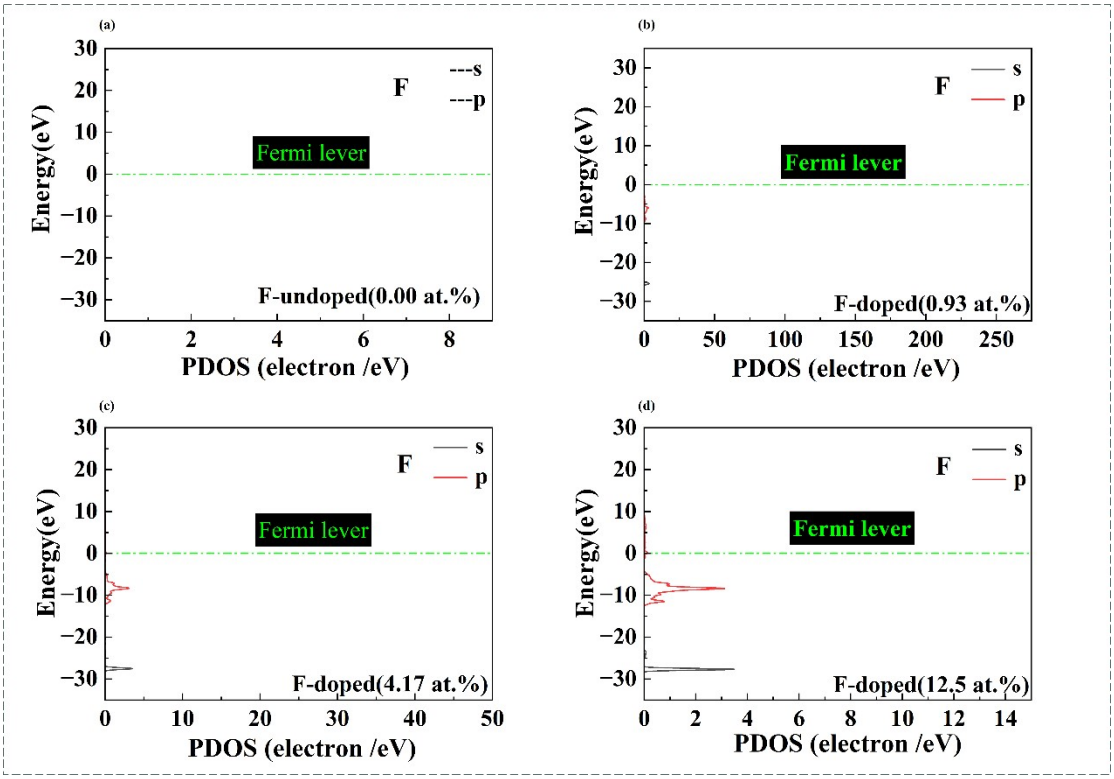

Fig. S9 F-PDOS

Supplementary Note 2

Experiment

Materials

The chemicals and reagents used in this experiment include: $PbBr_2$ (99%), CsBr (99%), ammonium fluoride (NH_4F), SnO_2 (99%), N,N′-Dicyclohexylcarbodiimide (DCC) (see Fig. S1), N,N-dimethylformamide (DMF, 99.9%), carbon tetrachloride (CCl_4, 99.9%), ethanol (99%), and isopropanol (≥99%). All reagents were purchased from Shanghai Macklin Biochemical Technology Co., Ltd. and were used without further purification.

Synthesis of SnO_2 Quantum Dots

0.8532 g anhydrous tin(II) chloride ($SnCl_2$) and 0.284 g thiourea were added together into a conical flask containing of 30 mL deionized water. The mixture was stirred continuously at room temperature for 36 hours until a pale yellow clear solution formed (see Fig. S2), and then allowed to stand for another 36 hours before further use.

Fabrication of HTMs-free carbon-based $CsPbBr_3$ PSCs

ITO glass substrates were sequentially ultrasonically cleaned in deionized water, ethanol, and isopropanol for 5 minutes each. They were then dried in an oven and treated with ozone for 10

minutes before use.

The electron transport layer (ETL) was fabricated via a spin-coating method. A SnO_2 quantum dot precursor solution was spin-coated onto the surface of a cleaned ITO substrate at 3000 rpm for 30 seconds, followed by annealing on a hotplate at 200 °C for 60 minutes to form the SnO_2 ETL layer.

The SnO_2/$CsPbBr_3$ interface modification layer was prepared as follows[1]. NH_4F solutions with different concentrations (0, 0.04, 0.06, and 0.08 M/L in deionized water) were spin-coated on the surface of SnO_2 film at 5000 rpm for 30 seconds, followed by annealing at 150 °C for 30 minutes. The corresponding samples were labeled as the control parameters 0.04-NH_4F, 0.06-NH_4F, and 0.08-NH_4F, respectively.

The $CsPbBr_3$ perovskite layer was prepared using a two-step method. First, a 1 M/L $PbBr_2$ solution (in DMF) was spin-coated on the surface of SnO_2 at 2000 rpm for 30 seconds onto the above ETL and then was heated at 90 °C for 30 minutes for Removing DMF solvent. Subsequently, a CsBr solution (2.5 g CsBr dissolved in 10 mL of a mixed solvent with V(water): V(isopropanol) = 9.5:0.5) was spin-coated on the surface of $PbBr_2$ film at 2500 rpm for 30 seconds, followed by final annealing at 250 °C for 5 minutes to obtain a dense and uniform $CsPbBr_3$ perovskite film.

The $CsPbBr_3$/C interface modification layer was prepared as follows[2],Solutions of DCC at different concentrations (0, 10, 20, and 30 mg/mL in dichloromethane) were spin-coated on the surface of $CsPbBr_3$ layer at 5000 rpm for 30 seconds, followed by annealing at 100 °C for 10 minutes to remove dichloromethane solvent. The corresponding samples were labeled as the control samples, 10-DCC, 20-DCC, and 30-DCC, respectively.

Finally, the conductive carbon paste was coated onto the surface of DCC modifying layer using a doctor-blade coating method. The electrode area was defined as 0.12 cm² through a shadow mask, and the device was heated at 100 °C for 15 minutes to complete the fabrication of the $CsPbBr_3$ perovskite solar cell.

Characterization Methods for Perovskite Solar Cells

Ultraviolet photoelectron spectroscopy (UPS) measurements were conducted under a bias voltage of 10 V. The J–V characteristics of the devices were tested using a xenon lamp light source to simulate AM 1.5G irradiation (100 $mW \cdot cm^{-2}$), with the effective testing area calibrated to 0.12 cm² using a mask. The voltage scanning range was set from 0.1 V to 1.7 V with a step size of 0.01 V, and a delay time of 0.04 s was applied. Electrochemical impedance spectroscopy (EIS) was performed on a AUTOLAB electrochemical workstation with a frequency range from 0.1 Hz to 3.92 MHz and an AC amplitude of 5 mV. The photoluminescence (PL) spectra of perovskite films were recorded with a fiber optic spectrometer (QE6500, Ocean Optics) using a 355 nm wavelength laser (0355–05–01–0020–700, Cobolt Zouk) as the excitation source.

Supplementary Note 3

Establishment of the dual-diode series model (DDSM).

（The parameters are defined as follows: V_1 and I_1 represent the voltage across diode D1 and the current flowing through it, respectively. V_2 and I_2 denote the voltage across diode D2 and the current flowing through it, respectively. I_{s1} and I_{s2} are the saturation currents of diodes D1 and D2, respectively; V_{D1} and V_{D2} correspond to the barrier heights of diodes D1 and D2, respectively. V and I indicate the applied voltage and current in the series circuit, respectively.）

$$I_1 = I_{s1}[e^{(qV_1/KT)} - 1] \quad (1)$$

$$I_2 = I_{s2}[1 - e^{(-qV_2/KT)}] \quad (2)$$

$$V = V_1 + V_2 \quad (3)$$

$$I_{s1} \propto e^{(\frac{-qV_{D1}}{KT})}, \ I_{s2} \propto e^{(\frac{-qV_{D2}}{KT})} \quad (4)$$

From the equation for series current ($I_1 = I_2$), we can obtain.

$$I_{s1}e^{\frac{qV_1}{KT}} - I_{s1} = I_{s2} - I_{s2}e^{\frac{-q(V-V_1)}{KT}} \quad (5)$$

The following formula is derived from (5).

$$e^{\frac{qV_1}{KT}} = \frac{I_{s1} + I_{s2}}{I_{s1} + I_{s2}e^{\frac{-qV}{KT}}} \quad (6)$$

Substituting into (1) yields.

$$I = I_1 = I_{s1}\frac{I_{s1} + I_{s2}}{I_{s1} + I_{s2}e^{\frac{-qV}{KT}}} - I_{s1} \quad (7)$$

$$I = I_{s1}\left(\frac{I_{s1} + I_{s2}}{I_{s1} + I_{s2}e^{\frac{-qV}{KT}}} - 1\right) = I_{s1}\left(\frac{I_{s1} + I_{s2} - I_{s1} - I_{s2}e^{\frac{-qV}{KT}}}{I_{s1} + I_{s2}e^{\frac{-qV}{KT}}}\right) \quad (8)$$

$$I = I_{s1}\frac{I_{s2} - I_{s2}e^{\frac{-qV}{KT}}}{I_{s1} + I_{s2}e^{\frac{-qV}{KT}}} \quad (9)$$

$$I = I_{s1}I_{s2}\frac{1 - e^{\frac{-qV}{KT}}}{I_{s1} + I_{s2}e^{\frac{-qV}{KT}}} \quad (10)$$

Supplementary Note4

The relationship between the $CsPbBr_3$/C interface barrier (eV_{D1}) and V_{OC}.

Since the interfacial barrier $eV_{D1} \gg eV_{D2}$, under an applied voltage V, the interfacial voltage satisfied $V_1 \gg V_2$. In other words, the applied voltage V was primarily distributed across diode D1 (interface $CsPbBr_3$/C) and was approximately equal to V_1. Combining equations (2) and (10), the I-V relationship satisfies.

$$I = I_1 \approx I_{s1}[e^{(\frac{qV}{KT})} - 1] \quad (11)$$

When $e^{\left(\frac{qV}{kT}\right)} \gg 1$, the I-V relationship satisfied.

$$I \approx I_{s1}e^{(\frac{qV}{KT})} \quad (12)$$

Under open-circuit conditions, the current satisfies $I = I_{sc}$, and $e^{\left(\frac{qV_{OC}}{kT}\right)} \gg 1$ (where V_{oc} was the open-circuit voltage, and I_{sc} is the photogenerated current.). Combining equations (4) and (12), the open-circuit voltage V_{oc} and the barrier height eV_{D1} satisfied the following relationship.

$$I_{sc} = Ce^{(\frac{-qV_{D1}}{KT})}e^{(\frac{qV_{OC}}{KT})} \quad (13)$$

$$e^{(\frac{qV_{oc}}{KT})} = \frac{I_{sc}}{C}e^{(\frac{qV_{D1}}{KT})} \quad (14)$$

$$V_{oc} = \frac{KT}{q}\ln\frac{I_{sc}}{C} + V_{D1} \quad (15)$$

The relationship between the barrier height eV_{D1} (q=e) and the Fermi level satisfied.

$$V_{\mathrm{D1}} = \frac{E_{f(CsPbBr3)} - E_{f\ (C)}}{q} \quad (16)$$

Combining equations (15) and (16), we could obtain.

$$V_{oc} = \frac{KT}{q}\ln\frac{I_{\mathrm{sc}}}{C} + \frac{E_{ef(CsPbBr3)} - E_{ef\ (C)}}{q} \quad (17)$$

Under the condition that the photogenerated current Isc and the Fermi level of carbon was unchanged, equation (17) simplifies to.

$$\Delta V_{oc} = \frac{\Delta V_{D1}}{q} = \frac{\Delta E_{ef(CsPbBr3)}}{q} \quad (18)$$

According to Equations (17) and (18), the V_{OC} was increased linearly with the increase of the eV_{D1}.

Supplementary Note 5

The relationship between the SnO_2/$CsPbBr_3$ interface barrier(eV_{D2}) and FF.

Under ideal conditions, when $V_1 \gg V_2$, the total voltage $V \approx V_1$, and the current -voltage characteristics of the device can be described by Equation (11).

In the actual system, however, the SnO_2/$CsPbBr_3$ interface induced a voltage V_2, so the current – voltage relationship was followed Equation (110).

$$I = \frac{I_{s1}I_{s2}\left(1-e^{-qV/kT}\right)}{I_{s1} + I_{s2}e^{-qV/kT}}$$

thereby deviating from the ideal diode behavior. This deviation constituted a key factor responsible for the reduction in the FF of the device.

In the DDSM based on the C/ SnO_2/$CsPbBr_3$ structure, since the series currents were equal ($I_1 = I_2$), the interfacial voltage V_1 and V_2 satisfy the following relationship.

$$I_{s1}\left[e^{\frac{qV_1}{kT}} - 1\right] = I_{s2}\left[1 - e^{-\frac{qV_2}{kT}}\right], V = V_1 + V_2$$

When the Fermi level of SnO_2 was shifted relative to that of $CsPbBr_3$, according to the barrier relation $V_{D2} = \frac{E_{f,\mathrm{CsPbBr_3}} - E_{f,\mathrm{SnO_2}}}{q}$, the SnO_2/$CsPbBr_3$ interface barrier eV_{D2} increases correspondingly, leading to a decrease in the reverse saturation current I_{s2} (Equation (4)). In this series configuration, voltage V_1 was decreased while V_2 increasing, thereby reducing the FF.

When the eV_{D2} *was* small, the increase in V_2 was limited, and the FF was declined gradually. However, when the eV_{D2} was large, I_{s2} became extremely small, causing the current to approximately satisfy the saturation condition.

$$I_{s1}\left[e^{\frac{qV_1}{kT}}-1\right] \approx I_{s2}$$

Consequently, the I–V curve exhibited a pronounced "plateau" characteristic, manifesting as an "S-shaped" distortion that severely deviated from ideal diode behavior, leading to a sharp drop in the FF.

Table S2 SCAPS-1D parameter settings (original)[3, 4]

parameter	ITO	SnO2	CsPbBr3	C
thickness(nm)	500	450	800	
E_g[eV]	3.5	3.6	2.3	
X[eV]	4	4.0	3.6	
ε_r	9	9	6.5	
N_C[cm^{-3}]	2.2×10^{18}	4.36×10^{18}	4.94×10^{17}	
N_V [cm^{-3}]	1.8×10^{19}	2.52×10^{19}	8.47×10^{18}	
μ_n[cm2/Vs)]	20	20	4500	
μ_p[cm2/Vs)]	10	10	4500	
NA[cm^{-3}]				
N_D[cm^{-3}]		2.0×10^{19}	1.0×10^{15}	
Workfunction(eV)				5

Table S3 Simulation of CsPbBr3/C barrier (Set the electron affinity (X) of CsPbBr3 to the parameters in the following table, with other parameters remaining the same as in the original table data)

X	4.0ev	3.9ev	3.8ev	3.7ev	3.6ev	3.5ev	3.4ev
$CsPbBr_3$/C	0.8396eV	0.939eV	1.039eV	1.139eV	1.239eV	1.339eV	1.439eV

Table S4 Simulation of SnO_2/$CsPbBr_3$ barrier (Set the electron affinity (X) of SnO_2 to the parameters in the following table, with other parameters remaining the same as in the original table data)

X	3.8ev	3.9ev	4.0ev	4.1ev	4.2ev
SnO_2/$CsPbBr_3$（eV_{D2}）	0eV	0.08eV	0.18eV	0.28eV	0.38eV

Table S5 Voltage division at the SnO_2/$CsPbBr_3$ interface.

eV_{D2}	0	0.08187557	0.18167470	0.28153164	0.38141575
eV'_{D2}	0	0.08187741	0.18171391	0.2831724	0.41718307
V_2	0	0.00000184	0.00003921	0.00164076	0.03576732

Table 4 shows the interface voltage division V_2 at the SnO2/CsPbBr3 interface when the applied voltage is 1.34V (the open-circuit voltage value). The V_2 values in the table are derived from the following relationship:

$$V_2 = \frac{eV'_{D2} - eV_{D2}}{e}$$

(In the formula, $eV_{D2}$and eV'_{D2}represent the SnO2/CsPbBr3 interface barrier potentials when the applied voltage V is 0 and 1.34, respectively.)

[1] Jung E H, Chen B, Bertens K, Vafaie M, Teale S, Proppe A, Hou Y, Zhu T, Zheng C, Sargent E H (2020) Bifunctional Surface Engineering on SnO2 Reduces Energy Loss in Perovskite Solar Cells. ACS Energy Letters 5:2796-2801. http://dx.doi.org/10.1021/acsenergylett.0c01566.

[2] Zhu J, Liu Y, He B, Zhang W, Cui L, Wang S, Chen H, Duan Y, Tang Q (2022) Efficient interface engineering of N, N'-Dicyclohexylcarbodiimide for stable HTMs-free CsPbBr3 perovskite solar cells with 10.16%-efficiency. Chemical Engineering Journal 428. http://dx.doi.org/10.1016/j.cej.2021.131950.

[3] Zhao P, Lin Z, Wang J, Yue M, Su J, Zhang J, Chang J, Hao Y (2019) Numerical Simulation of Planar Heterojunction Perovskite Solar Cells Based on SnO2 Electron Transport Layer. ACS Applied Energy Materials. http://dx.doi.org/10.1021/acsaem.9b00755.

[4] Baro M, Borgohain P (2025) Design and performance analysis of [formula omitted] perovskite solar cells: Insights from SCAPS-1D device simulations. Renewable Energy. http://dx.doi.org/10.1016/j.renene.2025.124225.